


Shear-assisted contact aging of single-asperity nanojunctions

Matthias Vorholzer ¹, Dirk Dietzel ^{1,2}, Ebru Cihan ^{1,3} and André Schirmeisen ^{1,2,*}

¹*Institute of Applied Physics (IAP), Justus-Liebig-Universität Giessen, 35392 Giessen, Germany*

²*Center for Materials Research, Justus-Liebig-Universität Giessen, 35392 Giessen, Germany*

³*Institute for Materials Science, TU Dresden, 01062 Dresden, Germany*

 (Received 9 December 2021; revised 10 March 2022; accepted 21 March 2022; published 2 May 2022)

Contact aging, i.e., the strengthening of a tribological contact with time, is a phenomenon that is commonly attributed to an increase of the effective contact area between multiasperity surfaces based on contact mechanical processes. Only recently, atomic force microscopy experiments and simulations on single silica nanojunctions have also demonstrated logarithmic aging with contact time for single-asperity contacts and the effects were attributed to a gradual formation of chemical bonds in the contact, thereby suggesting an atomistic mechanism of “contact aging.” Generally, this atomic bond-formation process is considered as a shear-assisted thermally activated process, where both temperature and loading conditions are expected to influence the aging behavior. A direct link between aging and temperature has recently been substantiated by temperature-dependent aging experiments and complementary molecular dynamics simulations, but the potential influence of shear stress on single-asperity aging still remains largely elusive. To analyze the role of shear stress, we now apply a simple and semianalytical model for thermally activated bond formation, which explicitly considers the reduction of energy barriers by a shear-stress-related Eyring term. Based on this model, characteristic fingerprints of mechanical shear can be identified in our temperature-dependent contact aging experiments, including, for instance, the counterintuitive decrease of aging effects with increasing temperature. Our results thereby hint at a path to introduce this form of qualitative contact aging to the phenomenological rate and state friction, where the local aging effects might be closely linked to the shear-stress distribution within multiasperity contacts.

DOI: [10.1103/PhysRevB.105.195401](https://doi.org/10.1103/PhysRevB.105.195401)

I. INTRODUCTION

Contact aging is a phenomenon well known for almost all macroscopic systems. Its effect becomes most apparent for the case of a stationary contact between a substrate and a slider, where the force required to initiate sliding usually increases logarithmically with the time. The commonly accepted view of contact aging revolves around the ubiquity of small-scale roughness, leading to patches of true contact at an interface, known as asperities [1,2]. In this picture, contact aging is then associated with an increase of the number of contact points and/or their overall contact area [3–5]. Based on this concept, phenomenological frameworks like, e.g., rate and state theories can describe macroscale friction dynamics reasonably well [6–8] with contact mechanical aspects, for instance, related to shear-induced creep, often being considered predominant for the aging process [5,9–12].

At the same time, a growing number of experimental and theoretical studies have recently highlighted the occurrence of nanoscale contact aging for single asperities of constant size [13–28]. Especially for silica junctions, as, e.g., formed between the sharp tip of an atomic force microscope (AFM) and the oxide layer of a Si wafer, interaction and aging dynamics have received considerable attention and already early publications have allowed one to correlate molecular dynamics (MD) simulations showing a gradual formation of

chemical bonds, i.e., siloxane bridges, at the interface [25,26] to the logarithmic aging behavior observed for static friction in AFM experiments at room temperature and under ambient conditions [13,14].

Such an atomistic aging mechanism by interfacial bond formation can be anticipated to be a thermally activated, mechanochemical process, where an effective energy barrier needs to be overcome for bond formation [15–17,25,29]. From a fundamental point of view as well as for bridging the gap between aging of single asperities and macroscopic rough contacts [27,30] it is then relevant to understand in more detail how temperature and loading conditions can affect aging of single-asperity nanojunctions.

The temperature dependence of contact aging for silica nanocontacts under ultrahigh vacuum (UHV) conditions was systematically analyzed in a recent study, where the prurture contact stiffness was used as a measure to quantify the contact strength after a defined hold time [23]. Here, both the experiments and the complementary MD simulations considering Si-O and Si-Si bonds verified the thermally activated character of the aging mechanism, which mainly became manifest in a linear increase of the bond-formation rate with temperature, i.e., $\dot{N} \propto T$, with N being the number of bonds at the interface, as theoretically predicted by Liu *et al.* (see Ref. [25], Supplemental Material).

In addition, also the influence of mechanical stress has been addressed in recent works. By considering stress-induced energy barrier changes in the vicinity of already

*schirmeisen@ap.physik.uni-giessen.de

formed bonds, MD simulations could rationalize how the experimentally observed fast aging rates can be reconciled with the assumed timescales for a gradual bond-formation scenario [25]. Beyond that, normal forces exerted by an AFM tip were considered as a possible factor to drive aging. However, a direct load dependence of the bond-formation rates could not unambiguously be identified and experimentally observed differences in aging were rather attributed to changes of the effective contact area between the tip and the sample [14].

Similarly, a shear-stress dependence of the aging dynamics can also be anticipated for single-asperity contacts, and in a previous study, the initial number of bonds after short aging times was tentatively linked to temperature-dependent shear-stress variations during aging [23].

This hypothesis is now used as a starting point for a more thorough discussion of the influence of shear stress on the aging behavior based on experiments for silica-silica and silica-diamond contacts. By combination of experiments and theoretical calculations we can then substantiate the surprising results of an initial contact stiffness that increases linearly with decreasing temperature. Although this behavior is seemingly incompatible to the concept of thermally activated bond formation, we discuss how this effect can be understood by considering the different loading conditions during the hold phase of our experiments. Determined by the temperature-dependent sliding friction [31,32], low temperatures result in high shear stress during the hold time, whereas higher temperatures lead to a reduced shear stress. We find agreement with the experiments using our semianalytical model that includes an energy barrier for bond formation modified by a shear-stress-related Eyring term [33], similar to load and shear-stress effects in nanoscale wear experiments [34–37].

II. EXPERIMENTAL APPROACH

The experimental data discussed in this work was obtained using a variable-temperature atomic force microscopy (VT-AFM) by Omicron under UHV conditions at a base pressure of $p < 5 \times 10^{-10}$ mbar [23]. The AFM was operated in contact mode. In this mode, the cantilever tip is sliding across the surface and torque related to friction between tip and surface induces a cantilever torsion that can be measured by laser-beam reflection [38].

We employed a slide-hold-slide protocol [13] as detailed in a previous publication [23], which allowed us to quantify the increased contact stiffness after a hold time t_{hold} .

To this end, friction loops of 300 nm in length were recorded, while the movement was interrupted in the middle of each forward or backward motion for a predefined hold time t_{hold} . Since the motion of the tip is interrupted in the middle of each scan, we can avoid larger tilts of the cantilever, which are inevitable at the end of each scan line and were found to potentially influence the results by introducing larger changes in contact geometry and shear stress [24]. Instead, the length of our friction loops was selected in such a way that stable sliding friction levels are reliably achieved and could be obtained by averaging over the last 20 nm before the stopping point. These sliding friction levels can then be identified as the

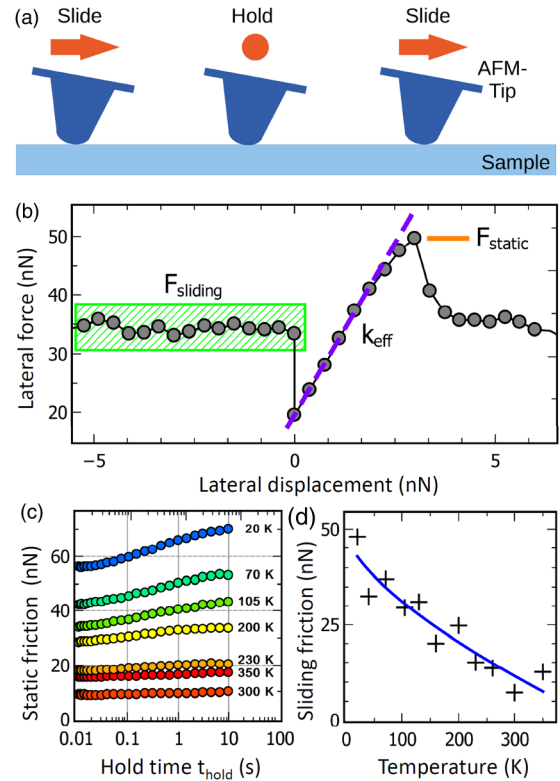


FIG. 1. (a) Schematic representation of the slide-hold-slide (SHS) approach, where scanning is suspended for a defined hold time t_{hold} before it is reinitiated. During t_{hold} , the cantilever torsion leads to shear stress acting on the interface. (b) Exemplary result from a SHS experiment for a silica tip on silica at 40 K for a hold time of 4.6 s. Several quantities around the stopping point (at $x = 0$) are evaluated. Sliding friction is averaged over several nanometers before stopping the tip. Static friction is the peak height after the hold. The effective contact stiffness corresponds to the lateral force buildup between the aforementioned parameters. (c) Aging as seen in the static friction (some curves are excluded for clarity). (d) Sliding friction corresponding to the static friction shows a clear temperature dependence and is fitted with a standard curve for thermally activated friction ($v = 2.5 \mu\text{m/s}$).

shear stress acting on the interface when the tip movement is halted.

When reinitiating sliding after t_{hold} , both the static friction and the effective contact stiffness k_{eff} can be recorded. The static friction is obtained from the peak in the lateral force F_L shortly after the hold time (Fig. 1). A relatively high scan speed of $2.5 \mu\text{m/s}$ is used throughout all of our experiments in order to minimize the effects of the thermally activated, gradual rupture of the contact, which must nonetheless be considered to affect the temperature and hold time dependence of the static friction that is exemplarily shown in Fig. 1(b). As a result, analyzing the static friction is not necessarily ideal to understand the interface processes, which are superimposed by the bond-breaking process. Nonetheless, already the static friction values hint at increased contact aging, i.e., the strengthening of the contact between the tip and the sample with time, for lower temperatures and

thus motivate the analysis based on the interfacial contact stiffness.

In Fig. 1(b), a decrease of the lateral force can be observed directly before the cantilever movement is reinitiated. This decrease can be correlated to a creeplike relaxation of the cantilever tip during the initial stage of each holding time t_{hold} [23]. After that, the gradient dF_L/dx until the static friction is reached can be identified as the contact stiffness. However, since a slight bend in the slope of the lateral force signal can be seen shortly before the static friction peak is reached, only the first 30% of each slope is taken into account. By confining our analysis to the beginning of the lateral force buildup for k_{eff} it is thus ensured that quantifying the aging process is decoupled from the gradual rupture of the contact. In this case, the effective contact stiffness k_{eff} can directly be interpreted as proportional to the number of bonds N , each of which has an average spring constant, k_{avg} , resulting in $k_{\text{eff}} = Nk_{\text{avg}}$ if the interfacial bonds are viewed as a system of springs in parallel [23]. In this picture, the torsional stiffness of the cantilever is not considered since it is higher by at least a factor of 4 than the contact stiffness between the tip and the sample. In the linear spring system formed by the cantilever and the contact, it is thus of negligible influence.

Ultimately, the contact stiffness can be considered as a particularly suitable measure for contact aging, and any calculation which can provide information on the number of bonds formed at the interface can directly be compared to the experimental results.

All experimental results were obtained using either standard Si cantilevers (PPP LFM, Nanosensors, Switzerland) or cantilevers terminated by a single crystal diamond (ADC-H-V0, Adama Innovations, Ireland), both with a nominal spring constant of 0.2 N/m, and lateral force signals were calibrated using the method introduced by Bilas *et al.* [39]. As samples, we analyzed oxide layers on Si(111) wafers. To remove residual water and physisorbed adsorbates, samples and tips were heated to 250 °C for 3 h under UHV conditions before the measurements. The slide-hold-slide experiments have been performed at different temperatures and the temperature sequence was randomized with frequent reference measurements at 300 K.

To improve the signal-to-noise ratio of the contact stiffness values, repeated measurements of the hold time dependence have been performed at each temperature. To this end, a line was first scanned repeatedly, while the hold time t_{hold} was first systematically increased from 10 ms up to the maximum value of about 2 s and then decreased back to 10 ms. Afterwards, the tip was shifted by 80 nm orthogonally to the scan line and a new set of hold-time-dependent slide-hold-slide measurements was recorded at this new position. Each data point for a given hold time t_{hold} was thus averaged over at least 50 individual observations of the contact stiffness, which keeps the influence of inherent fluctuations to a minimum (see also Ref. [23] for further details on the experimental procedure).

During the repeated back and forth scanning, wear of the surface can occur, predominantly at very low temperatures. Such measurements with discernible wear are usually omitted from the analysis, but exemplary curves are discussed later on in the context of aging of silica interfaces.

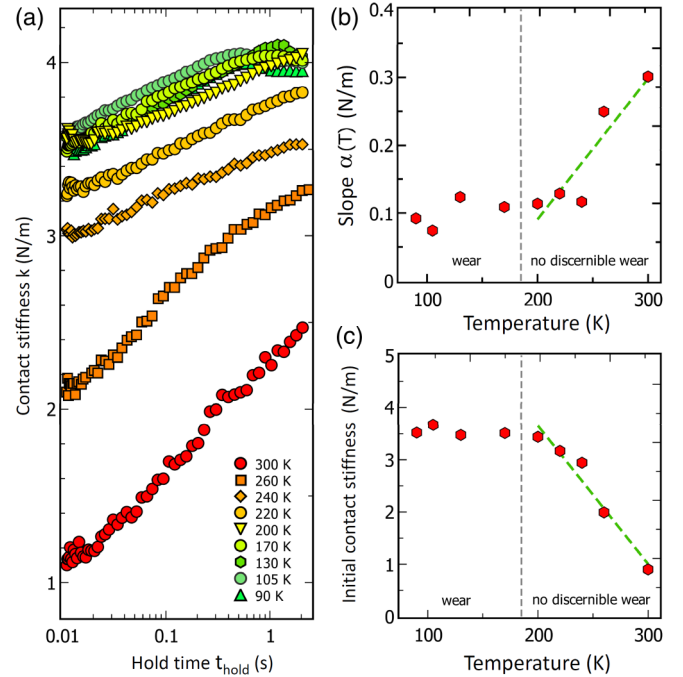


FIG. 2. Slide-hold-slide experiments for silica interfaces under UHV conditions. (a) Temperature and hold time dependence of the interfacial contact stiffness. (b) The temperature dependence of the resulting slope $\alpha(T)$ [cf. Eq. (1)] is shown as red spheres. (c) Temperature dependence of the initial contact stiffness $k_0(T)$ (red spheres). The vertical gray lines in panels (b) and (c) separate two regimes in which surface wear effects were or were not discernible. In the wear-free regime ($T \geq 200$ K) the quantities $\alpha(T)$ and $k_0(T)$ can well be described by a linear dependence on the temperature as indicated by the dashed green lines.

III. RESULTS AND DISCUSSION

A. Contact aging of silica interfaces

To discuss the influence of shear stress on the aging process, we first revisit experiments on silica interfaces [23], where logarithmic aging of the interfacial contact stiffness was observed during temperature-dependent slide-hold-slide experiments [Fig. 2(a)]. To consider also wear effects, Figs. 2 and 1 now encompass an extended temperature range (compared to Ref. [23]), where temperatures below $T = 200$ K show first signs of wear.

Independent of these wear effects, the contact stiffness k can generally be well described by a logarithmic function [23,25] in the form of

$$k(t, T) = k_0(T) + \alpha(T) \ln(t/t_0). \quad (1)$$

Here, $k_0(T)$ indicates the minimum contact stiffness after the shortest hold time of $t_0 = 10$ ms, and $\alpha(T)$ is a temperature-dependent scaling factor that determines the slope of the curves. Figures 2(b) and 2(c) then show the temperature dependence of $\alpha(T)$ and $k_0(T)$.

For the wear-free regime, i.e., $T \geq 200$ K, we find that the two parameters can be well approximated by a linear dependence on the sample temperature before both $\alpha(T)$ and $k_0(T)$ become relatively constant in the low-temperature regime.

While the temperature dependence of $\alpha(T)$ has already been extensively discussed in a previous publication [23], one of the main goals of this work will now be to analyze how the seemingly unexpected linear decrease of the initial contact stiffness $k_0(T)$ with increasing temperature for $T \geq 200$ K can be linked to the varying shear conditions during the hold time.

B. Calculation of contact aging dynamics

To determine $\alpha(T)$ and $k_0(T)$ based on calculations, we apply a simple model that also allows us to consider the influence of the interface conditions on the aging dynamics. Thereby, we can develop an intuitive understanding of the aging processes that complements the insight based on microscopic MD simulations [23,25]. More specifically, we start with an approach as suggested by Liu and Szlufarska [25] that is then extended to describe more complex scenarios with shear stress acting on the interface and bond rupture during the hold time (for the latter please see Appendix C).

In this model, we consider contact aging as resulting from a single type of chemical bonds that can be described by a spring constant k contributing to the effective, overall contact stiffness as $k_{\text{eff}} = N \times k$, with N being the number of bonds at the interface. Independent of the exact interface conditions and material combinations, such a model can be used as a reasonable first approximation for all aging processes related to thermally activated bond formation and will later on also be considered for aging effects of silica/diamond interfaces.

To describe a bond-formation process based on Arrhenius reaction kinetics, we first assume a distribution of available reaction sites $A(E)$ for a given activation energy barrier E . The rate of interfacial bond formation $dN(E, t)/dt$ at a given energy E can then be described as

$$\frac{dN(E, t)}{dt} = f_0[A(E) - N(E, t)]e^{-E/k_B T}, \quad (2)$$

with f_0 being the attempt frequency, k_B being the Boltzmann constant, and T being the temperature. Equation (2) thereby considers the bond-formation rate as directly proportional to the number of remaining reaction sites $A(E) - N(E, t)$, while a potential temperature dependence of the attempt frequency is not explicitly considered.

This differential equation can be solved analytically as

$$N(E, t) = A(E) \left\{ 1 - \exp \left[-t f_0 \exp \left(\frac{-E}{k_B T} \right) \right] \right\}, \quad (3)$$

and Eq. (3) can then be used to calculate the absolute number of bonds $N(t)$ formed after a given hold time by integration over all possible values of energy barriers for bond formation:

$$N(t) = \int_0^\infty A(E) \left\{ 1 - \exp \left[-t f_0 \exp \left(\frac{-E}{k_B T} \right) \right] \right\} dE. \quad (4)$$

In Eq. (4), one key element to describe the aging process is the distribution of energy barriers $A(E)$. In principle, methods like molecular dynamics or density functional theory can consider very detailed and realistic distributions of $A(E)$ where effects of mechanochemical coupling can be considered on different length scales [25,29] with, e.g., the formation of bonds impacting energy barriers at surrounding

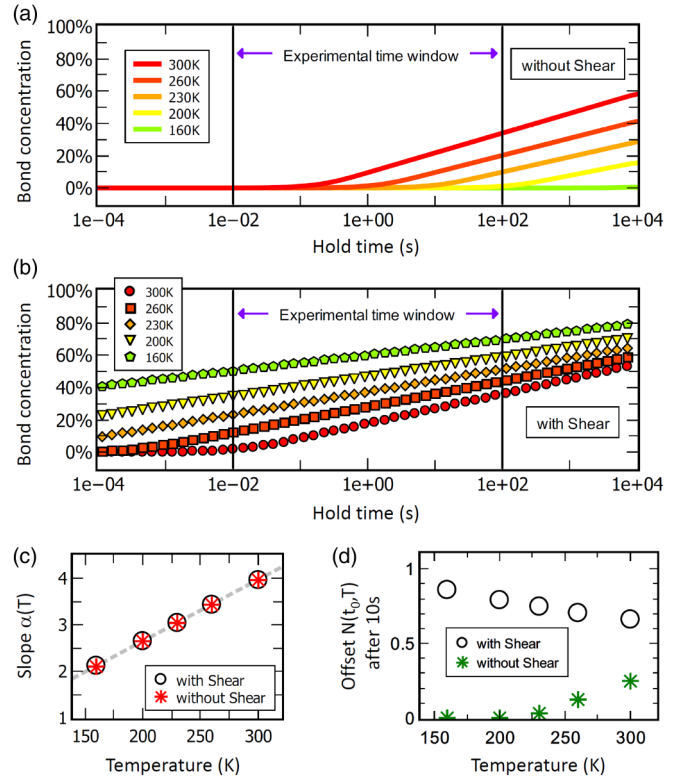


FIG. 3. The number of bonds calculated from Eq. (4) with a constant distribution $A(E)$ and an attempt frequency of $f_0 = 10$ MHz. (a) Excluding shear stress the outcome of a simple thermally activated process is visible. (b) When shear is included in the model the initial number of bonds is largest at low temperature while the slope remains unchanged. These curves show already a close resemblance of the experimental results for silica-silica interfaces. (c) The aging rate α is unaffected by shear stress and a linear dependency on temperature is found. (d) The temperature dependence of the offset k_0 at a fixed t_{hold} shows a slope reversal depending on whether shear stress is considered in the calculations.

reaction sites [25]. Ultimately, realistic interface conditions can, therefore, be extremely complex and cannot be captured by such a simple, semianalytical approach. However, as we show later on, the simplistic model is still able to describe fundamental trends of our temperature-dependent contact aging experiments, even if just a one- or two-level distribution for $A(E)$ is used.

1. Homogeneous distribution of activation energy barriers

To qualitatively explore the aging dynamics based on Eq. (4), we start with results obtained when using a constant distribution $A_1(E)$ between 0.75 and 1.3 eV [Fig. 3(a)]. As a first approximation, this range is aligned to the minimal and maximal bond-formation energies as reported for the case of siloxane bridges for silica interfaces [25]. However, the exact energy range does not alter the results qualitatively. As shown in Fig. 3 only a negligible amount of bonds is formed for short hold times, and higher temperatures lead to earlier and overall increased aging effects. While this result can be expected based on the concept of thermally activated bond formation and is perfectly in line with contact aging effects based on MD simulations [23,25], it is nonetheless not

reconcilable with the experimental results for contact aging of silica interfaces under UHV conditions [23], where lower temperatures resulted in a higher contact stiffness already after the minimum hold time of 10 ms.

In Ref. [23], this seemingly unexpected behavior was rationalized by considering that the friction force during sliding leads to an interfacial shear stress τ between the tip and the sample that is maintained when the tip is being stopped and effectively reduces the energy barrier for bond formation. Due to the typical temperature dependence of sliding friction [Fig. 1(d)], this effect is especially important for low temperatures, and the initial bond concentration after the minimum hold time might, thus, be higher than the bond concentrations for low temperatures.

To include the shear stress τ in the simplistic model, we now introduce an Eyring term to calculate an effective energy barrier for bond formation as $\Delta E_{\text{eff}} = \Delta E - \tau V_a$, with V_a being a characteristic activation volume [33]. The shear stress τ applied during the hold time is directly determined by the temperature-dependent sliding friction force $F_{\text{sliding}}(T)$ and the Eyring term can thus be expressed by $F_{\text{sliding}}(T)$ and a characteristic activation length l_A , which leads to $\tau V_a = F_{\text{sliding}} l_A$. In our calculations, we used characteristic activation lengths of $l_A = 20$ nm, while the temperature dependence of sliding friction corresponds to typical values obtained from the slide phases of our experiments, as, e.g., shown in Fig. 1. Here, the typical decrease of friction with temperature as described in the well-established theoretical models for thermally activated friction [31,32,40] can well be identified. For a more quantitative analysis, the effect of cantilever creep onto the shear stress might additionally be considered, but was not included in our qualitative considerations.

Figures 3(a) and 3(b) then show a direct comparison between the aging behavior calculated with and without an additional Eyring term, where the hold time range accessible to our experiments is additionally marked. We find that the aging process does not only start earlier when considering the effects of the interfacial shear stress but also the the slope of the bond concentration as a function of temperature at a given hold time t_{hold} reverses, exactly as observed in the experiments. This is illustrated in Fig. 3(d), which shows the relative number of bonds formed after a hold time of 10 s as a function of temperature. Without considering any effects of shear stress, this relative number of bonds increases as a function of temperature, while it decreases when the interfacial shear stress is considered as an influence on the effective energy barrier ΔE_{eff} . In principle, the reduction of energy barriers by the shear stress therefore overcompensates the generally less effective formation of bonds at lower temperatures by providing a larger pool of bonds that can be formed relatively easy. (Please note that for high shear stresses the effective energy barrier for certain bonds can be effectively zero, which means that this bond is assumed to form almost immediately.) In addition, Fig. 3(c) shows the slope $\alpha(T)$ of the logarithmic increase of the bond concentration $N(t, T) = N_0(T) + \alpha(T) \ln(t/t_0)$ that can be found in Figs. 3(a) and 3(b) for sufficient values of t_{hold} . We find that in both cases, the temperature-dependent slope scales as $\alpha(T) \propto T$ with no difference between the calculations with and without consideration of shear stresses.

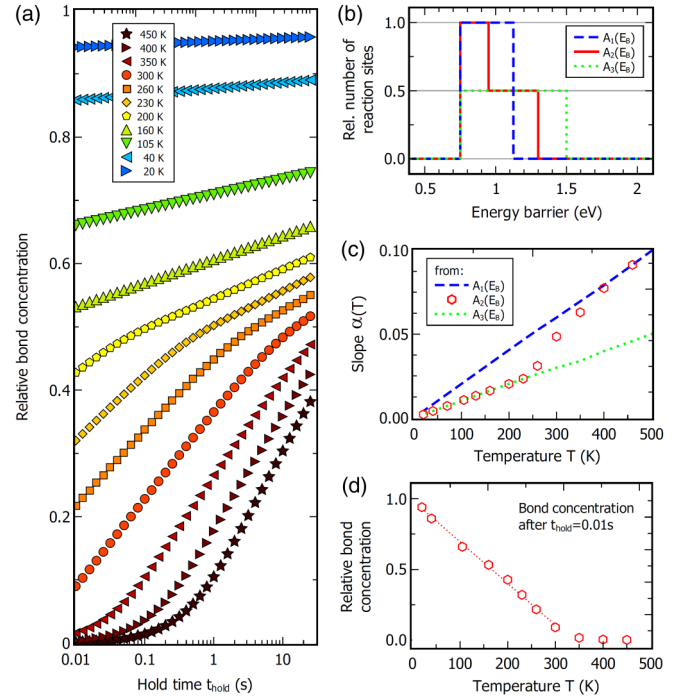


FIG. 4. Aging results calculated from Eq. (4) using a two-level distribution for $A(E)$. (a) Temperature and hold time dependence of the concentration of interfacial bonds. (b) Different distributions $A(E)$ that were used in the calculations. The blue dashed and green dotted lines each represent a simple high- or low-level distribution $A_1(E)$ and $A_3(E)$, while the solid red line represents $A_2(E)$ as used to calculate the concentration curves in panel (a). All three distributions include the same total number of reaction sites, which corresponds to 100% of the available bonds. (c) Average slopes of the logarithmic increase of bond concentration with hold time. The dotted and dashed lines represent the slopes α for the high- and low-level distributions $A_1(E)$ and $A_3(E)$, while the red hexagons represent the averaged slopes for $A_2(E)$ as determined from (a) between 0.05 and 1.2 s. (d) Temperature dependence of the relative bond concentration N_0 after the minimum hold time in panel (a).

2. Two-level distribution of activation energy barriers

In a second step, we have further improved this simple analytical model by introducing a more complex distribution for $A(E)$. In principle, implementing detailed distributions of available reaction sites as, e.g., for the case of siloxane bridges under ambient conditions [25], is possible. However, using a distribution that approximates the actual conditions by only including two levels of reaction site densities already allows us to better explore the impact on the aging dynamics. To this end, we now used a two-level distribution $A_2(E)$, which has a high density of available reaction sites from 0.75 to 0.95 eV and only half the density for energy barriers in the range from 0.95 to 1.3 eV [solid red curve in Fig. 4(b)]. Besides this two-level distribution for $A_2(E)$, we again described the shear stress effects by using temperature-dependent sliding friction values as exemplarily shown in Fig. 1(d). As further parameters we used an activation length of $l_A = 20$ nm, which is similar to the estimated tip radius, and a temperature-independent attempt frequency of 10 MHz within a hold time range of $0.01 \text{ s} < t_{\text{hold}} < 25 \text{ s}$.

Figure 4(a) then shows the hold time and temperature dependent aging dynamics for hold times of $10 \text{ ms} < t_{\text{hold}} < 25 \text{ s}$ and a temperature range between 20 and 450 K.

From Fig. 4(a) we find that the hold-time-dependent bond concentration curves can show two distinct slopes, which correspond to successive bond formation for the reaction sites with high and low densities. For each curve, an *average* slope α_2 has been determined for the hold time range of logarithmic increase of the relative bond concentration. The resulting temperature dependence of the slope $\alpha_2(T)$ is shown in Fig. 4(c) (red hexagons) in comparison to slopes obtained for uniform low- and high-level distributions as shown in Fig. 4(b) by the dotted and dashed lines.

In principle, $\alpha_2(T)$ still increases monotonously with temperature, but different regimes can directly be correlated to the two-level distribution $A_2(E)$. At low temperatures, the high shear stress is reducing the energy barriers significantly and a large number of bonds are already formed after the minimum hold time, resulting in a relatively low slope α . For high temperatures, the shear stress is much lower and consequently fewer bonds are formed within the minimum hold time and the high temperature allows for a quick formation of bonds from the high level of $A_2(E)$. In a transition regime, both the high- and low-level sections play a role, and consequently, slope changes can be observed in the hold time dependence of the bond concentration. In addition, Fig. 4(d) shows the temperature dependence of N_0 , which can be well approximated by a linear decrease for temperatures below 350 K and can be correlated to the initial contact stiffness $k_0(T)$.

3. Comparison to experiments

Despite the simplicity of the model to calculate the process of bond formation, the theoretical curves of Fig. 4 already describe the experimental results as, e.g., shown in Fig. 2 or in Ref. [23] quite well. This is true for the general trends of the aging curves as well as for the temperature dependence of $\alpha(T)$ and $k_0(T)$. (Please see also Appendix A for a direct side-by-side comparison between calculation and experiment in the relevant temperature range.)

The main indications for an influence of a nonhomogeneous distribution of energy barriers in our slide-hold-slide experiments are thus the following: First, the hold-time-dependent aging curves show slope changes in certain hold time and temperature ranges (Fig. 1 and Ref. [23]). Second, we find that the linear dependence on temperature of $\alpha(T)$ as, e.g., shown in Fig. 2(c) cannot be extrapolated to the coordinate origin. This becomes understandable when considering how a transition regime can influence the effective slope of $\alpha(T)$ within a limited temperature range.

In addition, Fig. 2 contains data curves obtained for low temperatures ($T < 200 \text{ K}$), where wear starts to play a role. Previously, it was unclear how these curves can fit into the general picture of contact aging. We now find that these temperatures mark a deviation from the theoretically anticipated trend of continuously increasing $\alpha(T)$ and decreasing $k_0(T)$. Instead both values become independent of temperature, which suggests that the interface conditions are changing and wear particles appear to be a limiting factor for further aging. As a result, these low temperatures can no longer be described by the simplistic model.

C. Contact aging for diamond on silica

To gain further insight into interfacial contact aging dynamics, we additionally analyzed an alternative material combination, where a diamond tip was used for slide-hold-slide measurements on a silica surface with the same experimental protocol as described in Sec. II.

In principle, also this system should be describable by the previously developed concepts, although the bond-formation process does involve different types of atoms and different distributions of activation energy barriers. Across the interface, both C-Si and C-O bonds are possible and have been previously examined with particular focus on wear effects between silica and diamond [41,42]. Numerical calculations have revealed a reduction in the binding energy at the interface, leading to the elongation of the Si-O and C-Si bonds which can result in bond breaking and even material transfer from silica to the diamond surface [42]. Furthermore, during wear of the diamond surface in contact with silica, the breaking process of C-C bond has been investigated through atomistic simulations [41]. It has been shown that O and Si pilot atoms can mechanochemically break the C-C bonds, due to the fact that C-O and C-Si bonds at the silica-diamond interface are strong enough to break a C-C bond on a defect-free diamond surface. However, for the case of our slide-hold-slide-experiments no discernible wear occurred for temperatures above 150 K, which suggests that the bond-breaking processes involve Si-C or Si-O bonds.

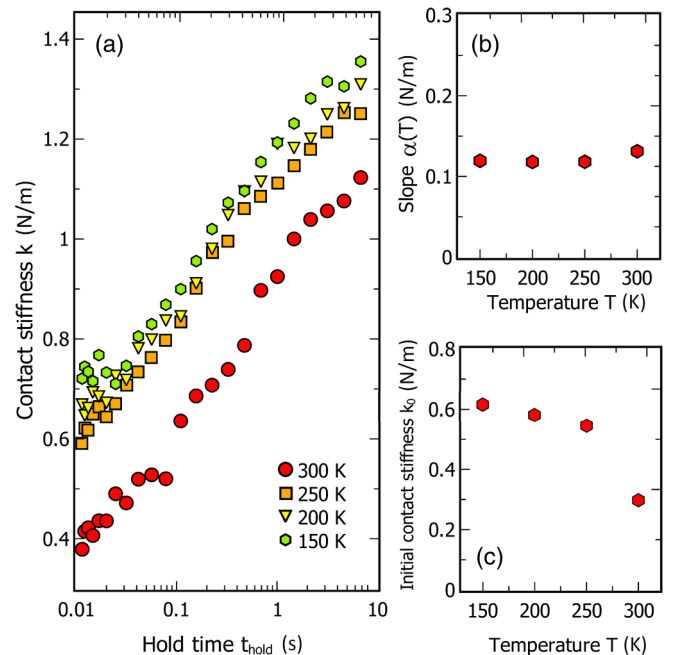


FIG. 5. Hold time and temperature dependence of the effective contact stiffness measured during slide-hold-slide experiments for a diamond tip on the oxide layer of a Si wafer. (a) A logarithmic strengthening of the contact stiffness is visible for each temperature. (b) All aging curves can be fitted with Eq. (1) and the resulting values of α (red hexagons) appear to be largely independent of T . (c) The initial contact stiffness after the minimum hold time (red hexagons) decreases with temperature.

Similar to Fig. 2(d) a continuous decrease of the sliding friction with increasing temperature has also been recorded for this interface. Figure 5(a) then shows the time and temperature dependence of the experimentally determined contact aging process and all curves can well be described by a logarithmic increase of contact stiffness with the hold time. In qualitative agreement with our previous considerations about shear-assisted contact aging we also find that the initial contact stiffness is increasing with decreasing temperature [Fig. 5(c)]. The slope $\alpha(T)$ [Fig. 5(b)], on the other hand, remains almost constant for temperatures above 150 K, i.e., in the wear-free regime, and an extrapolation to $T = 0$ K would yield a positive bond-formation rate.

Interestingly, a similar effect of an extrapolated nonzero bond-formation rate, albeit a negative one, could be observed for the transition regime of Fig. 4 between 200 and 350 K as a result of the specific two-level distribution of reaction sites $A_2(E)$. In the case of Fig. 5, the temperature-dependent slope α now suggests an increase of $A(E)$ with the energy barrier E . Then, the shear-stress-related shift of $A(E)$ makes higher densities of energy barriers available for bond formation at low temperatures but with a rate that is reduced by the temperature. A first approach to model this behavior would be to switch the high and low parts of $A_2(E)$ of Fig. 4 (see Appendix B).

IV. CONCLUSION

In conclusion, we analyzed the mechanisms of logarithmic contact aging [cf. Eq. (1)] through interfacial bond formation with special focus on the role of shear stress for the aging rates. As it turned out, considering an energy barrier distribution for bond formation modified by a shear-stress-related Eyring term is essential to reconcile the experimental results for temperature-dependent contact aging experiments with calculations based on thermally activated bond formation. In particular the aging dynamics for silica interfaces could well be described based on this approach, and in a further step, developing a model for the complex rupturing process might then give further insight into the technically relevant static friction forces, which are determined by both aging and rupturing.

The link between shear stress and initial contact stiffness is further corroborated by the temperature dependence of k_0 . Similar to the linear dependence of the slope $\alpha(T)$ on temperature, our calculations predict a linear decrease of the initial contact stiffness $k_0(T)$ with T , which is indeed found in the experiments. However, we have to keep in mind that this relation will depend on the distribution of available reaction sites $A(E)$, and strongly nonuniform distributions of the activation energy barriers might result in deviations from a simple linear decrease.

Nonetheless, the increase of k_0 with decreasing temperature must be considered as a characteristic fingerprint for a potential influence of the interfacial shear stress and was also found for experiments on silica-diamond interfaces. These results, therefore, also stress that at low temperatures the less efficient bond formation through thermal activation can be outweighed by the stronger reduction of energy barriers due to increased sliding friction and thus shear stress.

Still, we have to concede that the link between shear stress and aging is rather indirect since the shear stress is directly related to the sample temperature and these two influences are thus inevitably linked. Load-dependent measurements at a fixed temperature under UHV conditions might be a more direct approach for future experiments, but in this case load-dependent changes of the contact area need to be taken into account [14]. Alternatively, different shear stresses might be generated by varying the sliding velocity when approaching the hold position.

Ultimately, our study further emphasizes that nanoscale contact aging can be considered as a thermally activated process, where the bond-formation rates are also sensitively depending on the shear stresses acting at the interface. Especially this dependence on shear stress might be relevant for macroscopic models, since different shear stresses at the interface might not only influence the temporal evolution of the asperity population but also be of importance for their individual strength.

ACKNOWLEDGMENT

Financial support was provided by the German Research Foundation (Projects No. DI917/6-1, No. DI917/7-1, and No. DI917/8-1).

APPENDIX A: DIRECT COMPARISON BETWEEN EXPERIMENT AND THEORY

To better illustrate the correlation between the experiments and the theoretical calculations, we have prepared an additional figure (Fig. 6) which shows both the experimental results for silica contacts from Fig. 2(a) and the theoretical calculations from Fig. 4(a) in a side-by-side presentation. Figure 6 is limited to the experimentally accessible hold time

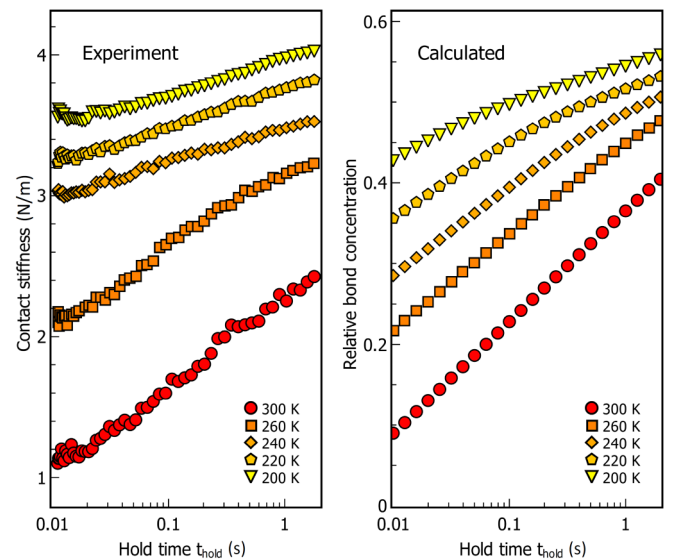


FIG. 6. Direct comparison between the results for temperature- and hold-time-dependent slide-hold-slide measurements of the contact stiffness for silica contacts (left panel) and theoretical calculations as detailed in Sec. III B (right panel).

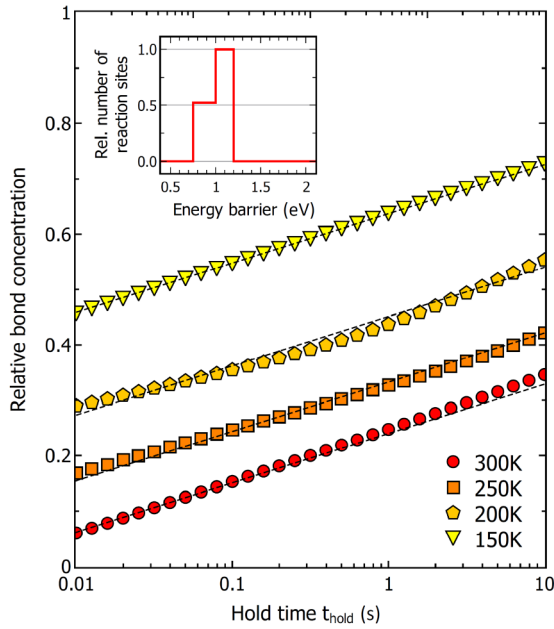


FIG. 7. Temperature and hold time dependence of the concentration of interfacial bonds calculated from Eq. (4) using a two-level distribution $A_{2^*}(E)$ as shown in the inset. The parallel dashed lines of the main figure illustrate that the slope $\alpha(T)$ is only weakly depending on temperature.

range and temperatures for which no discernible wear has been observed.

When comparing the two subfigures of Fig. 6 we have to consider that the experimentally observed contact stiffness does not decrease to zero, even for extremely short hold times. This offset in contact stiffness can be related to contact-mechanical effects or a small number of bond formation already occurring during continuous scanning [15–17]. Such an offset is not considered in the calculations, where a contact stiffness of $k = 0$ N/m is assumed as long as no bonds are formed.

APPENDIX B: REVERSE TWO-LEVEL DISTRIBUTION

In the main text, it was speculated that a first approach to explain the relatively constant values of $\alpha(T)$ for the diamond-silica system [Fig. 5(b)] might include a modified two-level distribution $A_{2^*}(E)$, where the relative number of reaction sites is initially low, but increases for higher energy barriers. Figure 7 now shows the effect of such a distribution on the aging dynamics and thereby illustrates a contact aging scenario, where the average slopes of the hold-time-dependent bond concentrations are only weakly depending on temperature.

In a simple picture, this can be understood based on the combined effects of shear stress and temperature: For low temperatures, the high shear stress makes a high concentration of reaction sites accessible, which are “harvested” rather slowly. For higher temperatures, bonds are generally formed faster, but due to the reduced shear stresses primarily regions with lower bond concentrations are contributing. The contact aging experiments thus allow us to develop a basic idea about the bond energy distribution. However, no further insight into

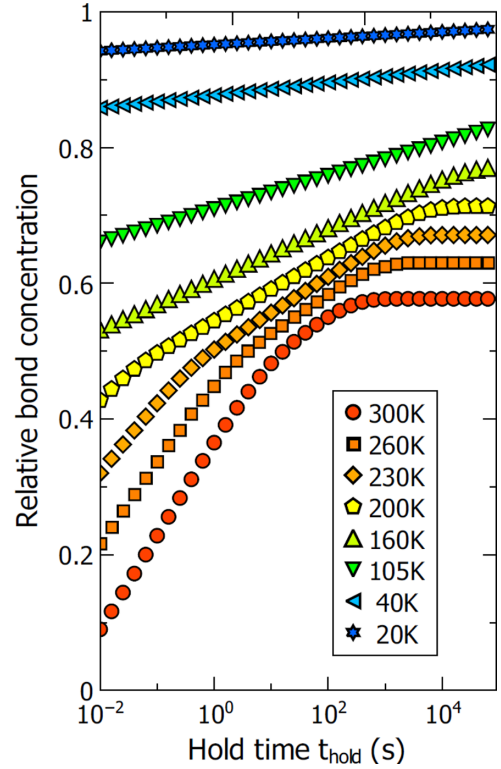


FIG. 8. Temperature- and hold-time-dependent aging results calculated from Eq. (C2) using the same two-level distribution $A_2(E)$ as used in Fig. 4 and a fixed energy barrier for bond rupture of 1.1 eV. A high probability for bond breaking is assumed, effectively prohibiting bond formation at energies above 1.1 eV.

the atomistic origins of this bond energy distribution can be gained at this point.

APPENDIX C: BOND RUPTURE DURING THE HOLD TIME

To explain our experimental results, considering bond rupture during the aging process has not been necessary, since good agreement between experiment and theory was already achieved by using a model that only considers bond formation. Nevertheless, bond rupture can easily be incorporated into this model. More specifically, Eq. (2) can be modified by adding a negative bond-formation rate to represent rupture.

Equation (2) then changes to

$$\frac{dN(E, t)}{dt} = f_0[A(E) - N(E, t)]e^{-E/k_b T} - f_1 N(E, t)e^{-E_r/k_b T}. \quad (C1)$$

Here, f_1 represents the attempt frequency for bond rupture, and the energy barrier to rupture a bond in a thermally activated process is represented by E_r . This differential equation can be solved analytically and the total number of bonds after a time t can be quantified as

$$N(t) = \int_0^\infty \frac{A(E)f_0 \exp(\varepsilon_r)}{f_0 \exp(\varepsilon_r) + f_1 \exp(\varepsilon)} \times \{1 - \exp[-t f_0 \exp(\varepsilon) - t f_1 \exp(\varepsilon_r)]\} dE, \quad (C2)$$

with $\varepsilon = E/k_b T$ and $\varepsilon_r = E_r/k_b T$.

Equation (C2) can then be solved numerically. This is illustrated in Fig. 8, where the calculations for shear-assisted contact aging as shown in Fig. 4 have been modified by also considering bond rupture with a constant energy barrier of $E_r = 1.1$ eV [43] and an attempt frequency of $f_1 = f_0 = 10$ MHz.

In Fig. 8, the influence of bond rupture can best be identified for long hold times and high temperatures. In this case, the relative bond concentration saturates below 100%, when an equilibrium between formation and

breaking is reached, while it would inevitably approach 100% without rupturing. In addition, we find that the curves for low temperatures ($T \leq 160$ K) are not significantly influenced by the process of thermally activated rupturing.

To first illustrate the general effect of bond rupturing on the aging process, we have not yet considered any potential influence of shear stress. Again, a possible approach would be to consider an energy barrier E_r reduced by a shear-stress-related Eyring term.

-
- [1] F. P. Bowden and D. Tabor, The area of contact between stationary and between moving surfaces, *Proc. R. Soc. London, Ser. A* **169**, 391 (1939).
- [2] J. Greenwood and J. Williamson, Contact of nominally flat surfaces, *Proc. R. Soc. London, Ser. A* **295**, 300 (1966).
- [3] J. H. Dieterich and B. D. Kilgore, Direct observation of frictional contacts: New insights for state-dependent properties, *Pure Appl. Geophys.* **143**, 283 (1994).
- [4] T. Baumberger and C. Caroli, Solid friction from stick-slip down to pinning and aging, *Adv. Phys.* **55**, 279 (2006).
- [5] R. Sahli, G. Pallares, C. Ducottet, I. E. B. Ali, S. A. Akhrass, M. Guibert, and J. Scheibert, Evolution of real contact area under shear and the value of static friction of soft materials, *Proc. Natl. Acad. Sci. USA* **115**, 471 (2018).
- [6] A. L. Ruina, Slip instability and state variable friction laws, *J. Geophys. Res.* **88**, 10359 (1983).
- [7] J. R. Rice and A. L. Ruina, Stability of steady frictional slipping, *J. Appl. Mech.* **50**, 343 (1983).
- [8] C. Marone, Laboratory-derived friction laws and their application to seismic faulting, *Annu. Rev. Earth Planet Sci.* **26**, 643 (1998).
- [9] P. Berthoud and T. Baumberger, Role of asperity creep in time- and velocity-dependent friction of a polymer glass, *Europhys. Lett.* **41**, 617 (1998).
- [10] B. N. J. Persson, O. Albohr, F. Mancosu, V. Peveri, V. N. Samoilov, and I. M. Sivebaek, On the nature of the static friction, kinetic friction and creep, *Wear* **254**, 835 (2003).
- [11] P. Berthoud, T. Baumberger, C. G'Sell, and J.-M. Hiver, Physical analysis of the state- and rate-dependent friction law: Static friction, *Phys. Rev. B* **59**, 14313 (1999).
- [12] S. Dillavou and S. M. Rubinstein, Shear Controls Frictional Aging by Erasing Memory, *Phys. Rev. Lett.* **124**, 085502 (2020).
- [13] Q. Li, T. E. Tullis, D. Goldsby, and R. W. Carpick, Frictional ageing from interfacial bonding and the origins of rate and state friction, *Nature (London)* **480**, 233 (2011).
- [14] K. Tian, N. N. Gosvami, D. L. Goldsby, Y. Liu, I. Szlufarska, and R. W. Carpick, Load and Time Dependence of Interfacial Chemical Bond-Induced Friction at the Nanoscale, *Phys. Rev. Lett.* **118**, 076103 (2017).
- [15] I. Barel, M. Urbakh, L. Jansen, and A. Schirmeisen, Multibond Dynamics of Nanoscale Friction: The Role of Temperature, *Phys. Rev. Lett.* **104**, 066104 (2010).
- [16] I. Barel, M. Urbakh, L. Jansen, and A. Schirmeisen, Temperature dependence of friction at the nanoscale: When the unexpected turns normal, *Tribol. Lett.* **39**, 311 (2010).
- [17] I. Barel, M. Urbakh, L. Jansen, and A. Schirmeisen, Unexpected temperature and velocity dependencies of atomic-scale stick-slip friction, *Phys. Rev. B* **84**, 115417 (2011).
- [18] M. Feldmann, D. Dietzel, H. Fuchs, and A. Schirmeisen, Influence of Contact Aging on Nanoparticle Friction Kinetics, *Phys. Rev. Lett.* **112**, 155503 (2014).
- [19] M. Feldmann, D. Dietzel, A. Tekiel, J. Topple, P. Grütter, and A. Schirmeisen, Universal Aging Mechanism for Static and Sliding Friction of Metallic Nanoparticles, *Phys. Rev. Lett.* **117**, 025502 (2016).
- [20] J. J. Mazo, D. Dietzel, A. Schirmeisen, J. G. Vilhena, and E. Gnecco, Time Strengthening of Crystal Nanocontacts, *Phys. Rev. Lett.* **118**, 246101 (2017).
- [21] M. Evstigneev, A. Schirmeisen, L. Jansen, H. Fuchs, and P. Reimann, Contact ageing in atomic friction, *J. Phys.: Condens. Matter* **20**, 354001 (2008).
- [22] N. N. Gosvami, M. Feldmann, J. Peguiron, M. Moseler, A. Schirmeisen, and R. Bennewitz, Ageing of a Microscopic Sliding Gold Contact at Low Temperatures, *Phys. Rev. Lett.* **107**, 144303 (2011).
- [23] M. Vorholzer, J. G. Vilhena, R. Perez, E. Gnecco, D. Dietzel, and A. Schirmeisen, Temperature Activates Contact Aging in Silica Nanocontacts, *Phys. Rev. X* **9**, 041045 (2019).
- [24] C. Petzold, M. Koch, and R. Bennewitz, Friction force microscopy of tribochemistry and interfacial ageing for the SiO_x/Si/Au system, *Beilstein J. Nanotechnol.* **9**, 1647 (2018).
- [25] Y. Liu and I. Szlufarska, Chemical Origins of Frictional Aging, *Phys. Rev. Lett.* **109**, 186102 (2012).
- [26] A. Li, Y. Liu, and I. Szlufarska, Effects of interfacial bonding on friction and wear at silica/silica interfaces, *Tribol. Lett.* **56**, 481 (2014).
- [27] S. Li, S. Zhang, Z. Chen, X.-Q. Feng, and Q. Li, Length Scale Effect in Frictional Aging of Silica Contacts, *Phys. Rev. Lett.* **125**, 215502 (2020).
- [28] R. Capozza, I. Barel, and M. Urbakh, Probing and tuning frictional aging at the nanoscale, *Sci. Rep.* **3**, 1896 (2013).
- [29] Z. Li and I. Szlufarska, Physical Origin of the Mechanochemical Coupling at Interfaces, *Phys. Rev. Lett.* **126**, 076001 (2021).
- [30] Z. Li, L. Pastewka, and I. Szlufarska, Chemical aging of large-scale randomly rough frictional contacts, *Phys. Rev. E* **98**, 023001 (2018).
- [31] E. Gnecco, R. Bennewitz, T. Gyalog, C. Loppacher, M. Bammerlin, E. Meyer, and H. J. Güntherodt, Velocity Dependence of Atomic Friction, *Phys. Rev. Lett.* **84**, 1172 (2000).
- [32] Y. Sang, M. Dube, and M. Grant, Thermal Effects on Atomic Friction, *Phys. Rev. Lett.* **87**, 174301 (2001).

- [33] H. Eyring, Viscosity, plasticity, and diffusion as examples of absolute reaction rates, *J. Chem. Phys.* **4**, 283 (1936).
- [34] P. Sheehan, The wear kinetics of NaCl under dry nitrogen and at low humidities, *Chem. Phys. Lett.* **410**, 151 (2005).
- [35] B. Gotsmann and M. A. Lantz, Atomistic Wear in a Single Asperity Sliding Contact, *Phys. Rev. Lett.* **101**, 125501 (2008).
- [36] Y. Shao, T. D. B. Jacobs, Y. Jiang, K. T. Turner, R. W. Carpick, and M. L. Falk, Multibond model of single-asperity tribochemical wear at the nanoscale, *ACS Appl. Mater. Interfaces* **9**, 35333 (2017).
- [37] W. Wang, D. Dietzel, and A. Schirmeisen, Thermal Activation of Nanoscale Wear, *Phys. Rev. Lett.* **126**, 196101 (2021).
- [38] C. M. Mate, G. M. McClelland, R. Erlandsson, and S. Chiang, Atomic-Scale Friction of a Tungsten Tip on a Graphite Surface, *Phys. Rev. Lett.* **59**, 1942 (1987).
- [39] P. Bilas, L. Romana, B. Kraus, Y. Bercion, and J. L. Mansot, Quantitative characterization of friction coefficient using lateral force microscope in the wearless regime, *Rev. Sci. Instrum.* **75**, 415 (2004).
- [40] L. Jansen, H. Hoelscher, H. Fuchs, and A. Schirmeisen, Temperature Dependence of Atomic-Scale Stick-Slip Friction, *Phys. Rev. Lett.* **104**, 256101 (2010).
- [41] A. Peguiron, G. Moras, M. Walter, H. Uetsuka, L. Pastewka, and M. Moseler, Activation and mechanochemical breaking of C-C bonds initiate wear of diamond (110) surfaces in contact with silica, *Carbon* **98**, 474 (2016).
- [42] A. Ciniero, G. Fatti, M. C. Righi, D. Dini, and T. Reddyhoff, A combined experimental and theoretical study on the mechanisms behind tribocharging phenomenon and the influence of triboemission, *Tribol. Online* **14**, 367 (2019).
- [43] Z. Li and I. Szlufarska, Multiphysics model of chemical aging in frictional contacts, *Phys. Rev. Materials* **2**, 063602 (2018).